NAVAL POSTGRADUATE SCHOOL

MONTEREY, CALIFORNIA

THESIS

FLOW VISUALIZATION STUDIES OVER A UCAV 1303 MODEL

by

CHUA, Weng Heng

June 2009

Thesis Advisor: M. S. Chandrasekhara

Approved for public release; distribution is unlimited

THIS PAGE INTENTIONALLY LEFT BLANK

REPORT DOCUMENTATION PAGE		*Form Approved OMB No. 0704-0188*
Public reporting burden for this collection of information is estimated to average 1 hour per response, including the time for reviewing instruction, searching existing data sources, gathering and maintaining the data needed, and completing and reviewing the collection of information. Send comments regarding this burden estimate or any other aspect of this collection of information, including suggestions for reducing this burden, to Washington headquarters Services, Directorate for Information Operations and Reports, 1215 Jefferson Davis Highway, Suite 1204, Arlington, VA 22202-4302, and to the Office of Management and Budget, Paperwork Reduction Project (0704-0188) Washington DC 20503.		
1. AGENCY USE ONLY *(Leave blank)*	**2. REPORT DATE** June 2009	**3. REPORT TYPE AND DATES COVERED** Master's Thesis
4. TITLE AND SUBTITLE Flow Visualization Studies over a UCAV 1303 Model		**5. FUNDING NUMBERS**
6. AUTHOR(S) CHUA, Weng Heng		
7. PERFORMING ORGANIZATION NAME(S) AND ADDRESS(ES) Naval Postgraduate School Monterey, CA 93943-5000		**8. PERFORMING ORGANIZATION REPORT NUMBER**
9. SPONSORING /MONITORING AGENCY NAME(S) AND ADDRESS(ES) N/A		**10. SPONSORING/MONITORING AGENCY REPORT NUMBER**
11. SUPPLEMENTARY NOTES The views expressed in this thesis are those of the author and do not reflect the official policy or position of the Department of Defense or the U.S. Government.		
12a. DISTRIBUTION / AVAILABILITY STATEMENT Approved for public release; distribution is unlimited		**12b. DISTRIBUTION CODE**
13. ABSTRACT (maximum 200 words) This study is a qualitative documentation of the main flow features that affect the aerodynamic performance under steady and unsteady maneuver conditions. The relevant fluid flow physics is not available presently and, hence, this thesis concentrated on generating those critical details. Towards this goal, model studies were conducted on the United States Air Force (USAF) geometry, described as same UCAV 1303, which is essentially a flying wing in the Naval Postgraduate School (NPS) water tunnel using dye-flow visualization technique. This study adapted the UCAV model 1303 for the NPS water tunnel by incorporating multiple ports for dye injection and was manufactured using rapid prototyping techniques. To obtain conditionally sampled flow images, especially for unsteady flow conditions, special phase locking circuitry was designed, fabricated and integrated with high resolution digital cameras and tunnel flow monitoring software. Flow visualization images at various Reynolds numbers, model attitudes and pitch rates were obtained. Strong vortical flow was observed as expected for a 47 degree delta-wing. The shallow sweep angle and tail-less geometry seemed to present some unusual aerodynamic characteristics in regard to vortex bursting.		
14. SUBJECT TERMS Unsteady Aerodynamics, UCAV Maneuvers, 2D-unsteady flows		**15. NUMBER OF PAGES** 59
		16. PRICE CODE
17. SECURITY CLASSIFICATION OF REPORT Unclassified	**18. SECURITY CLASSIFICATION OF THIS PAGE** Unclassified	**19. SECURITY CLASSIFICATION OF ABSTRACT** Unclassified	**20. LIMITATION OF ABSTRACT** UU

NSN 7540-01-280-5500

Standard Form 298 (Rev. 2-89)
Prescribed by ANSI Std. 239-18

THIS PAGE INTENTIONALLY LEFT BLANK

FLOW VISUALIZATION STUDIES OVER A UCAV 1303 MODEL

CHUA, Weng Heng
ST Dynamics Pte Ltd
B.Eng (Hons)., University of Newcastle

Submitted in partial fulfillment of the
requirements for the degree of

MASTER OF SCIENCE IN MECHANICAL ENGINEERING

from the

**NAVAL POSTGRADUATE SCHOOL
June 2009**

Author: CHUA, Weng Heng

Approved by: Professor M. S. Chandrasekhara
                 Thesis Advisor

                 Professor Knox T. Millsaps
                 Chairman, Department of Mechanical and Astronautical
                 Engineering

THIS PAGE INTENTIONALLY LEFT BLANK

ABSTRACT

This study is a qualitative documentation of the main flow features over an Unmanned Combat Air Vehicle (UCAV) 1303 model by flow visualization techniques where it gives the first understanding of the UCAV maneuverability under steady and unsteady maneuver conditions. The relevant fluid flow physics is not available presently and, hence, this thesis concentrated on generating those critical details. Towards this goal, model studies were conducted on the United States Air Force (USAF) geometry, described as same UCAV 1303, which is essentially a flying wing in the Naval Postgraduate School (NPS) water tunnel using dye-flow visualization technique. This study adapted the UCAV model 1303 for the NPS water tunnel by incorporating multiple ports for dye injection and was manufactured using rapid prototyping techniques. To obtain conditionally sampled flow images, especially for unsteady flow conditions, special phase locking circuitry was designed, fabricated and integrated with high resolution digital cameras and tunnel flow monitoring software. Flow visualization images at various Reynolds numbers, model attitudes and pitch rates were obtained. Strong vortical flow was observed as expected for a 47 degree delta-wing. The shallow sweep angle and tail-less geometry seemed to present some unusual aerodynamic characteristics in regard to vortex bursting.

THIS PAGE INTENTIONALLY LEFT BLANK

TABLE OF CONTENTS

THIS PAGE INTENTIONALLY LEFT BLANK

LIST OF FIGURES

x

ACKNOWLEDGMENTS

THIS PAGE INTENTIONALLY LEFT BLANK

I. INTRODUCTION

A. DESCRIPTION OF WORK

The operational requirements of next generation Unmanned Combat Air Vehicle (UCAV) demand many complicated maneuvers. Being a pilotless vehicle, it allows performing such maneuvers that are not generally permitted for a piloted aircraft. Mission requirements for such UCAVs include reliably performing varieties of combat roles, such as flying surveillance missions, strike and suppression of enemy air defenses, attack of both fixed and maneuvering targets, routine take-off from and return to carrier decks. For successful design and operation, a thorough and basic understanding of the flow field over such configurations is required.

Since present fluid flow physics knowledge over maneuvering UCAVs does not exist readily, the objective of this thesis is to qualitatively document the main flow features over a UCAV 1303 model using the methodologies of flow visualization. The successful interpretation of these fluid flow patterns is an important tool used in the investigation and studies of the physics behind the complex three-dimensional eddying motion and turbulence. Flow visualization provides the first insight on the UCAV maneuverability by observing the location and time of vortex bursting in relations to aerodynamic lift under steady and some unsteady conditions.

Model studies were conducted on the United States Air Force (USAF) geometry - UCAV 1303 [1, 2] in the Naval Postgraduate School (NPS) water tunnel using dye-flow visualization technique. This geometry is currently being evaluated by the USAF in various wind tunnels and computational studies with many researches in steady flows. Thus, unsteady aerodynamics knowledge of the same configuration will add to the knowledge base on the geometry and enable better designs. The geometry, in particular, uses a shallow sweep angle delta wing, without vertical tails with a cranked trailing edge. These features lead to many unique flow features, especially the formation and bursting of the well-known delta wing leading edge primary vortices that actually enable the delta

1

wing to produce large lift coefficients. The bursting process of these vortices is of great interest in this case because it is notably affected by the absence of a vertical tail.

B. FLOW OVER A DELTA WING: MECHANICS OF VORTEX DEVELOPMENT AND BURSTING

For delta wings undergoing a positive angle of attack, it is well known that, due to flow separation on the surface during flight, two rotating vortices in the opposite directions are created by the leading edge of the wing. Flow that was originally attached on the lower surface at modest angle of attack turns outward at severe turning and approaches the leading edge when flow separates and developed. Due to the difference in pressure from the lower and upper surfaces of the delta wing, a primary vortex is created on both sides of the upper wing when the shear layer rolls-up and moves inward. The vortex axis is positioned approximately above the lifting surface at one vortex core diameter in slender wings and nearer to the surface for wings that are non slender.

These rotating leading vortices at the edges caused increased flow velocities, and as a result, according to Bernoulli theorem, cause low static pressure regions. This produces large suction forces near to the leading edge on the surface, which generates an additional lift commonly known as vortex lift. The loss of leading edge suction, due to flow separation, causes a small increase in drag. At high angles of attack, these vortices cause a delta wing to generate the advantage of additional vortical lift, which further push the stall angle of attack, resulting in a good maneuverability for a larger range of angles of attack.

The primary vortex core is approximately circular region of high vorticity with an axisymmetric flow. The flow in the vortex cores looks like a rotating jet [3]. The vortex core diameter increases linearly along the downstream, and it results in the conical shape of the vortical region. This conical structure is enclosed by a complex three-dimensional unsteady flow. The vortex flow is highly unsteady, with a maximum of time averaged axial velocity which is larger than the freestream flow velocity. As a result of the interaction between the primary vortices and the boundary layer, secondary vortices are brought on by lateral flow towards the leading edge under the primary vortex cores.

2

Outboard movement of the primary vortex at the surface boundary layer encounters an adverse pressure gradient, which causes it to separate and form a secondary vortex. Secondary vortices, which are smaller, tend to have a vorticity of opposite sign and collapse faster than primary vortices. Secondary vortices produce an inward displacement of the primary vortices to a greater effect, if the boundary layer is laminar. This is because the flow separation occurs faster and the secondary vortices are bigger. There may also be higher order vortical structures between the primary and secondary vortices [4].

C. ANGLE OF ATTACK

The typical features of the vortices developed on a delta wing are clearly dependent on the angle of attack of the wing. When it increases,

1. The strength and size of the vortex increase [5].

2. The inclination angle of the vortex path, with respect to the wing surface, increases linearly. For this reason, the plane containing the two vortex cores moves away from the wing surface [5].

3. The location of vortex collapse moves forward on the chord in the direction of the apex of the wing. This movement reduces the surface where the vortex suction forces are, and as a result induces lift losses on the back of the wing [5].

4. With increasing angle of attack, these fluctuations become more significant [5].

5. In particular, at low Reynolds number, the path of the vortices is sensitive to angle of attack with inboard movement at increasing angle of attack. This sensitivity to angle of attack decreased at high Reynolds number [5].

6. The presence of local separation over the main wing, and also the control surfaces, thus makes aircraft control difficult.

D.   REYNOLDS NUMBER AND MACH NUMBER

The structure of the vortex is especially sensitive to the Reynolds number. This is an important consideration, since the Reynolds number (Re $\approx 10^4$) for water tunnel is about two orders of magnitude below the Reynolds number (Re $\approx 10^6$) of a typical wind tunnel and about three to four orders of magnitude below the Reynolds number (Re $\approx 10^7$ to 10^8) for flight [5]. Nonetheless, if the flow separates from a sharp edge, it is likely to be much less sensitive to changes in the turbulent regime.

A low Reynolds number means the influence of viscosity is increased. This explains the consequence of a change in Reynolds number. For a 50° delta wing with sharp edges, the vortex structure is sparse at low Reynolds number (Re = 4,300), and it becomes denser with an increase of Re [3]. The maximum jet velocity in the vortex core increases with Reynolds number [4]. At Re = 8,700, a typical vortex collapse was observed and a secondary vortex structure forming outboard of the primary vortex could be observed [3, 4, 6]. This secondary vortex observed at higher Re undergoes collapse more upstream than the primary vortex, and it is possible that it starts the primary vortex breakdown [6]. When the Reynolds number increases, the leading edge vortices collapse sooner. The vortices path is shifted outboard and the angle between the vortex core axis and the wing surface increases. In addition, the transition from coherent to collapse vortices seems less sudden when Re increases, with a spiral mode at low Re and a form of collapse unclear at high Re.

When the Reynolds number increases past 30,000, the flow achieves an asymptotic state and becomes nearly independent to Reynolds number. For such high Reynolds numbers, the collapse of the vortex occurs near to the peak, even at small angle of attack of a few degrees. Results such as these validate the current lower Reynolds number study. For the experiments previously mentioned, the Reynolds number was modified by changing the velocity, and so an increase of the Reynolds number came with an increase of the Mach number. In the experiment by Luckring [7], the temperature could be increased so as to increase the local speed of sound and keep the Mach number

constant. As a result, the effects of Mach number and Reynolds number could be studied separately in his experiment, whereas in the other experiments [3, 8, 9], it was not possible to distinguish their respective effects. With Re = 6 x10^7 separation occurred at 13° instead of 11° with Re = 6 x10^6, and the suction coefficient was 80% higher for the higher Re [5]. The Reynolds number sensitivity seems to be partially eliminated when using a sharp leading edge, which can be explained by the fact that the sharp edge forces the separation at the leading edge. In fact, it is this feature that justifies the present test as well.

The Mach number of the flow establishes the importance of the compressibility effects, and also has a great affect on the vortex development. An increase in the Mach number leads to more considerable instabilities and hence to an earlier vortex collapse. These results are confirmed by Luckring [7], who found that an increase of the Mach number between 0.4 and 0.6 promotes leading edge separation.

E.   UNMANNED COMBAT AERIAL VEHICLE

1.   Design of UCAV 1303

The designs of a typical aircraft, where all the considerations and requirements related to the human crew are no longer limitations, are not the same as the design of a UCAV. All systems that are associated to the pilots, such as ejector seat, environmental control system, canopy and display devices are no longer necessary. As a result, with more functional space, the UCAV design can be lighter. The aerodynamic and stealth considerations are given a greater influence on the designed shape since the performance and maneuverability of the UCAV are no longer referenced from human tolerance to high acceleration but on the engine and airframe structural parameters. Different from conventional aircraft, UCAV can be employed in high risk environments without threat to life where their life cycle and operating costs are lower as well.

Woolvin [1, 2] has evaluated the performances of three configurations of 30 (aspect ratios 6.7), 47 (aspect ratios of 3.8) and 60 (aspect ratios 2.0) degrees. The general shape was flying wings without tail where propulsion is generated by a single engine

placed on the UCAV centerline. One of the significant interests of flying wings is to present a low observability, rather than maneuverability, and consequently a better survivability. Indeed without a tail, the radar cross section is significantly lower, which means that the aircraft is stealthier and hence, its survivability greatly improved. Moreover, aircraft without a tail is aerodynamically efficient, with low drag, and the engine integration is easier. The drawbacks are the difficulties in providing directional stability and control from an entirely horizontal lifting surface, and an increased tendency to side-slip. The longitudinal control is also limited due to the short moment arm of the elevators. Hence, the maneuver capability is limited. A solution to overcome the absence of horizontal or vertical tail is to use split ailerons or drag rudders and a thrust vectoring nozzle to provide yaw control [1, 2]. One of the major challenges with the development of flying wings is to understand the flight control systems associated with these configurations. With the 1303 and its "lambda" shape, there is an additional problem because the flow tends to separate over the outboard wing and therefore over the trailing edge devices installed here [5].

High leading edge sweep angle shapes have better stealth properties and result in favorable drag characteristics at supersonic speeds. One interest of the trailing edge cranks is that the radar cross section is minimized when the trailing edge use the same sweep angle as the leading edge, or when the trailing edge is aligned with the leading edge of the opposite side of the wing. Moreover, several components, such as the engine, fuel tanks, weapons bays and undercarriages, have to be fitted in the flying wing, and the crank angles allow the accommodation of all the components within a reduced area resulting in a lighter and stealthier UCAV. And lastly, the trailing edge control surfaces (ailerons, drag rudders), which are used for the three longitudinal, directional and lateral controls are more efficient at an appropriate sweep angle.

These UCAV were first sized using Defense Science and Technology Laboratory's air vehicle Conceptual Design and Optimization program, in order to obtain a minimum basic mass empty. The basic mass empty is defined as the sum of structure, propulsion and equipment masses [10]. Basic mass empty estimation is critical, especially when a new project starts and usually very little information is available to the

engineer, but nevertheless an estimated value is required [11]. According to Woolvin [1, 2], basic mass empty is used as the "figure of merit," which is minimized in the conceptual design process because, at a given 'technology level', basic mass empty is seen as having a direct influence on vehicle procurement cost. The scale of the engine could be modified according to the needs. The propulsion system had a minimum length, which is responsible for the shape of the 47° and 30° wings, which are over-sized in order to fit the engine. As a result, these vehicles were using only 50% of the volume available for fuel. The designed aircraft has to meet a number of requirements, such as a reasonable center of gravity position, a maximum take-off distance to reach a 50 feet screen height, the ability to carry enough fuel for the mission radius required, and the ability to achieve a minimum specific excess power at $M = 0.8$ at sea level. It is expected the 30° wing has highest lift over drag ratio, and the 60° wing has the lowest. However, the 47° wing has the best results with the lower basic mass empty for the whole radius range. The basic mass estimation increases with the mission radius. This was expected because in order to carry more fuel, a more powerful engine was needed. The 60° and 47° wings were limited by the take-off distance requirement, and the 60° wing could not reach the higher mission radii, whereas the 30° wing was limited by the specific excess power requirement. The 30° wing is much heavier than the other wings because it is too oversized, and so even if the lift over drag ratio is lower, the drag is too large and necessitates a heavy engine to reach the thrust requirement.

Therefore, for the requirements imposed, the 47° wing has the lower basic mass empty. The 60° wing has also a low basic mass empty but a limited mission radius, and the 30° wing is too heavy unless the specific excess power requirement is relaxed.

2   Modifications of UCAV 1303 Model

The basic UCAV shape, which is used in this thesis, is a thin flat model established on the 1303 shape. The 1303 is a single engine UCAV with 47° leading edge sweep and +/- 30° and +/- 47° trailing edge sweep [1]. As already stated, this shape had the best basic mass empty for the Defense Science and Technology Laboratory study [1]. The 1303 was first developed by the US Air Force Research Laboratory.

Using SolidWorks® to re-design the given 3-D CAD of the 1303 prototype (Figure 1), building the model by rapid prototyping process and common workshop tools, the modifications made to the given prototype are the overall scale down of the given 1303 prototype from 13" wind-span to 9" (Figure 2), modifications of the given 1303 prototype from dye passage to the dye tubes (Figure 3) and the re-design of the sting assembly to fit onto the C-strut model support of the NPS water tunnel (Figure 4 and Figure 5).
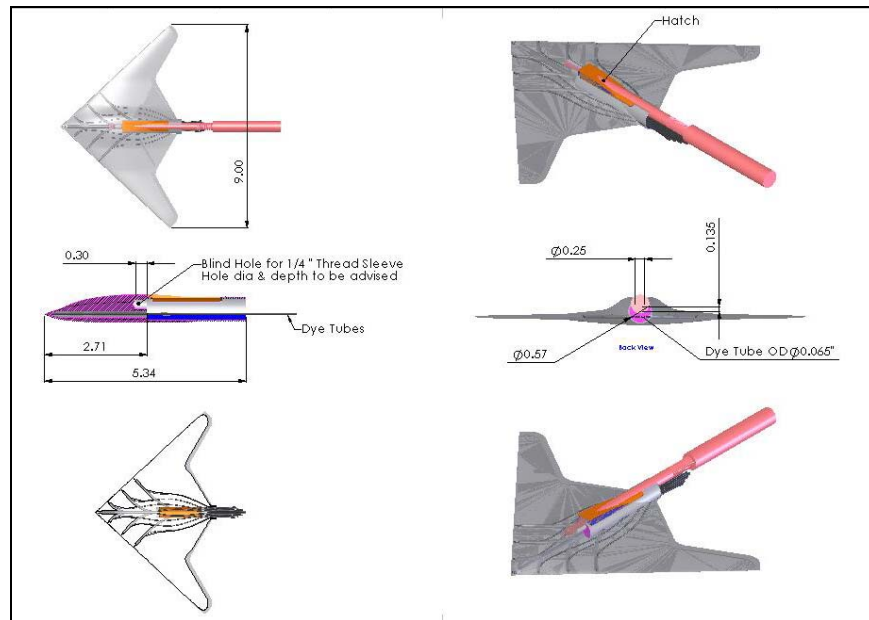
Figure 1.　Three-dimensional modeling of UCAV 1303 using SolidWorks®
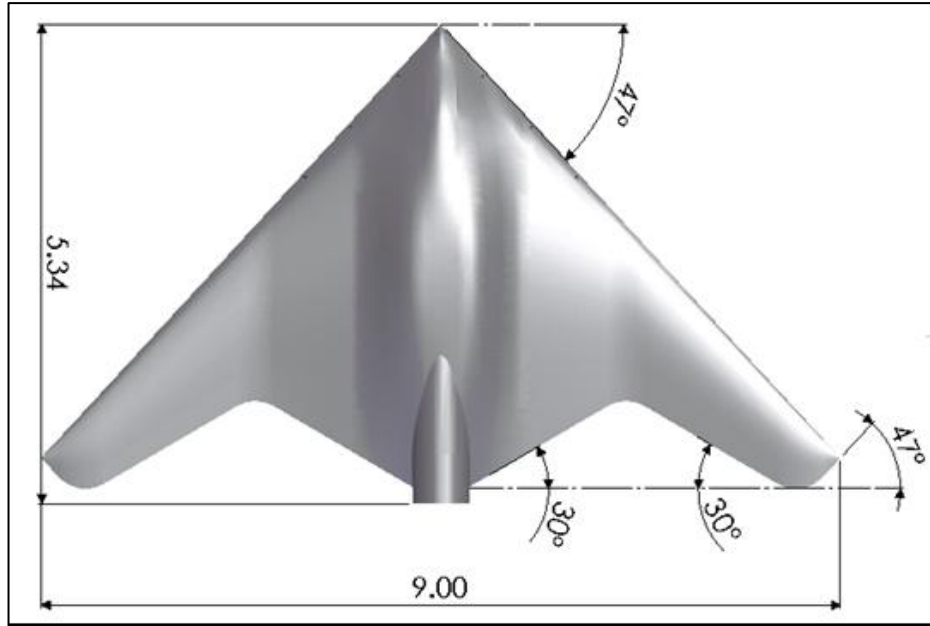
Figure 2.   Dimensions of UCAV 1303model used in NPS water tunnel
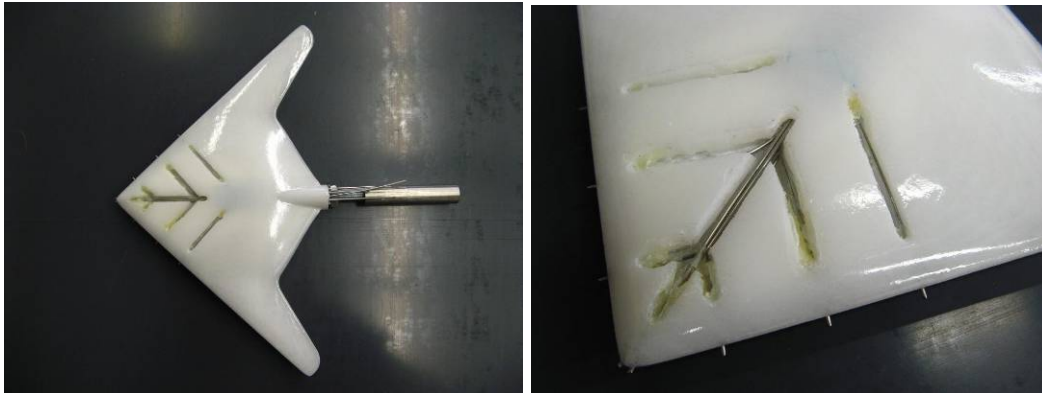
Figure 3.   Dye tubes modifications of UCAV 1303 model used in NPS water tunnel
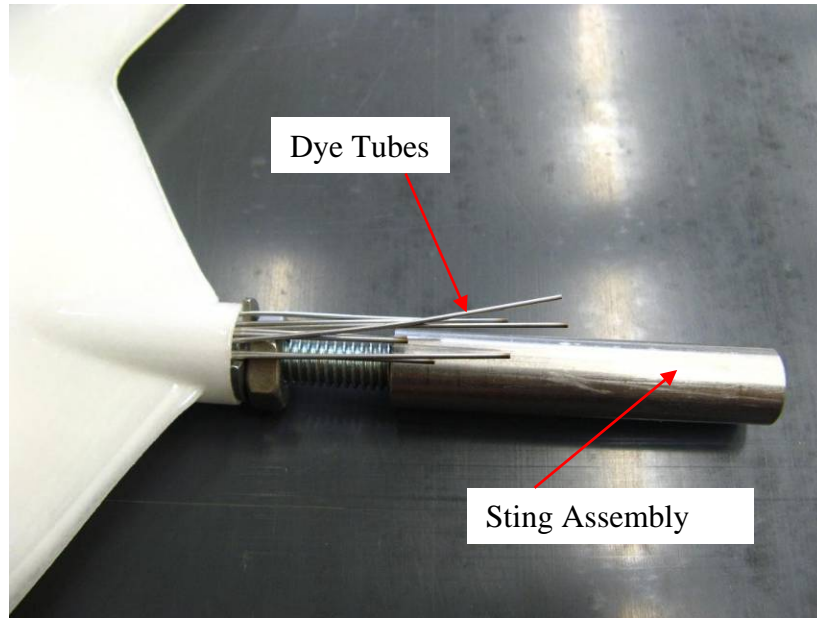
Figure 4.   Sting assembly of the modified UCAV 1303 prototype
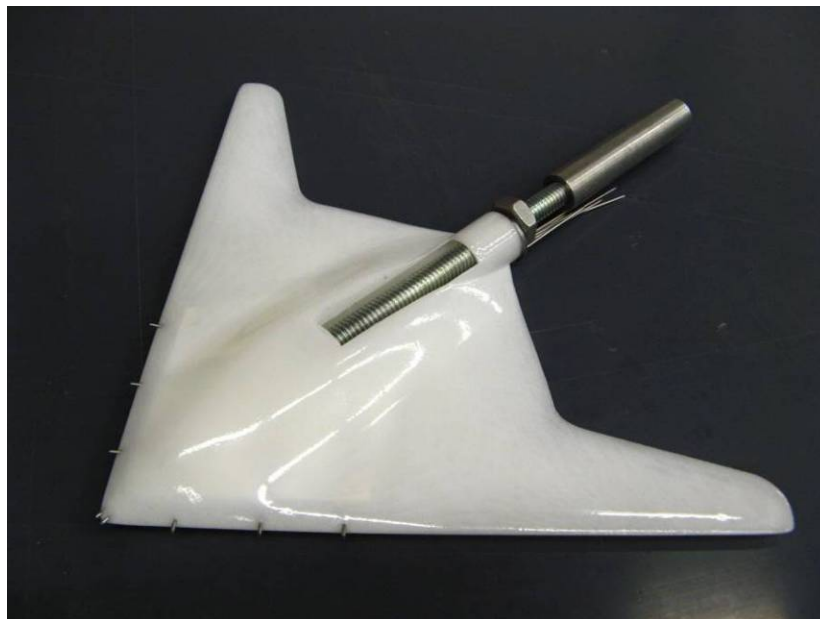
Figure 5.   Perspective view UCAV 1303 showing sting assembly

From literature searches, previous studies have shown that the aerodynamic performance [12] for Mach numbers from 0.45 to 1.4, in the Boeing Polysonic Wind Tunnel, for a range of angle of attack from -2° to 20°. This upper value was too small to observe the stall, lift loss and nose-up pitching moment [12].   In addition, the 1303

aerodynamic performances have been evaluated by Qinetiq [13], as well, in a low speed wind tunnel between Mach, M = 0.13 to 0.30 and with reference to the mean aerodynamic chord, the Reynolds numbers, Re = $3.1x10^6$ to $8.5x10^6$. A number of shapes, like baseline, sharp, and rounded shapes were studied [14]. The lift coefficient increases linearly till approximately 9° angle of attack, and then there is a slight reduction in the slope because of the increasing scale of flow separation on the upper-side of the wing. The maximum lift coefficient is achieved at about 20°.

With Mach number increase, compressibility effects cause an earlier vortex collapse and the flow separates more inboard. An increase of the Reynolds number causes a delayed vortex bursting due to the transition line moves forward on the chord, and the turbulent boundary layer is more resilient to separation. Transition bands were not use, unlike the U.S. Air Force Research Laboratory model, and so the level of the laminar flow was not possible to be determined. This effect was constrained with sharp leading edges where well-established leading edge vortex (LEV) flows were possibly present.

The baseline design is neutrally stable until about 9° angle of attack (or 6° with a sharp leading edge), and then a strong pitch up is seen due to the development of the LEV and the loss of lift at the back. At about 16°, the pitch up reverses as the LEV collapse and the pressure increases on the windward side near from the trailing edge. At around 23° angle of attack, the pitching moment turns negative [5]. Since a flying wing has a restricted longitudinal control power, the pitch up point at first instances is possibly to be the upper limit of the flight envelope. It is clear that the complex aerodynamics of this plan form needs to be studied and properly understood in great detail over a range of flow conditions, if superior operational functionality is to be derived from its use.

THIS PAGE INTENTIONALLY LEFT BLANK

II.   METHOD OF APPROACH

A.   NPS 15" × 20" FLOW VISUALIZATION TUNNEL

The NPS 15" × 20" water tunnel is a closed circuit facility suitable for studying a wide range of aerodynamic and fluid dynamic phenomena. The facility is operated as a continuous flow channel. Its key design features are high flow quality and horizontal orientation. The horizontal configuration provides easy model access, enables the model to be readily set-up without draining the water from the tunnel. The test section is constructed mainly of glass to permit maximum viewing of the model that allows simultaneous viewing from the top, bottom, both sides and from the rear. Photography is setup through the bottom and sides of the test section.

Figure 6.   NPS 15" x 20" Flow visualization water tunnel

1.   Model Support

The NPS 15" × 20" flow visualization water tunnel model support system utilizes a C-strut to vary the pitch angle and a turntable to vary the yaw angle. The model support includes the capability to perform motions in the roll axis. The roll mechanism

consists of one main cylindrical support that attaches to the C-strut. The cylindrical support houses a DC gear motor and an encoder. The roll mechanism is water-proofed and has a moisture detection system in case water leaks inside the support. If moisture or water is detected, a red light will go on at the tunnel front panel. The range of motion of the large C-Strut is limited from 0° to 40° when the roll mechanism is installed. The C-strut and the turntable are driven by remotely-controlled electric DC motors and the pitch and yaw angles are displayed in digital form. The C-strut arrangement permits continuous pitch motions up to 50° between the limits of -10° and 110°. This is accomplished by a sliding C-strut/sting assembly that allows the initial pitch angle to be set at -10° and in 15° increments from 0° to 60°. From any initial pitch angle, motor-driven angular motions of up to 50° are allowed. Angles of attack from 10° to -110° are achieved by rolling the model 180° around the sting. The turntable normally provides ±30° in yaw. The entire model support is lifted off the top of the test section during experimental set-up. The UCAV 1303 model is accessed by rotating the model support platform on hinges attached to a permanent base plate about a horizontal axis perpendicular to the test section centerline.
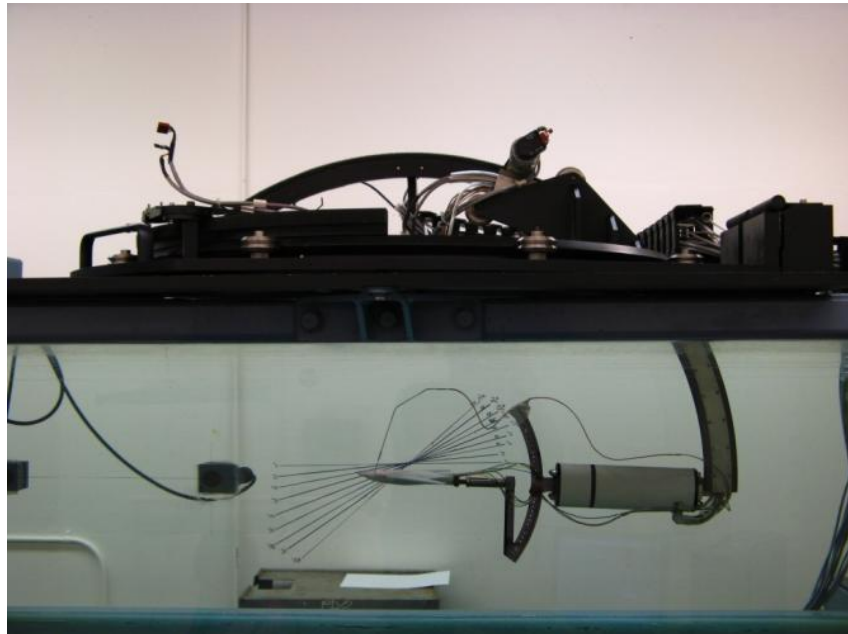

Figure 7.   Mounting of UCAV 1303 onto NPS 15" × 20" water tunnel

2.   Motion Control

With the inclusion of position feedback in the motor drive controller, the NPS 15" × 20" flow visualization water tunnel is able produce high-resolution motions with minimum vibration or undesirable unsteadiness. The water tunnel model support is equipped with a DC permanent magnet planetary gear motors with HP incremental optical encoders. The 24 volt motor, which is also used in the roll mechanism, has a gear ratio of 36:1, and provides a maximum speed of 5,700 rpm at no load and a maximum continuous torque of 102 in-oz. The HP encoder, which has a resolution of 512 cycles per revolution, provides the required position feedback to obtain accurate motions in the three axes. The motors installed in the model support are shown in Figure 8.
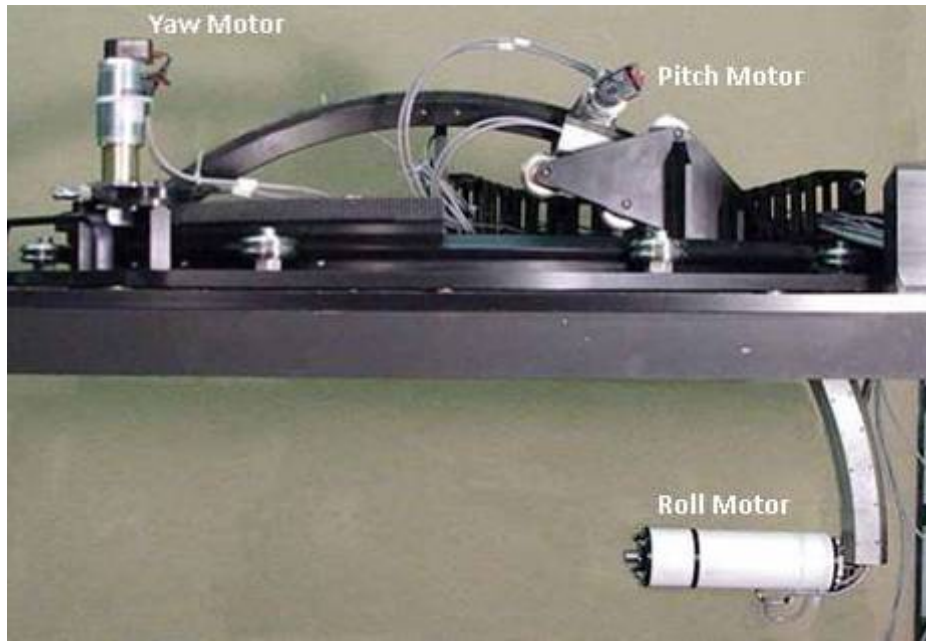

Figure 8.   Yaw, pitch and roll motors of the NPS 15" × 20" water tunnel

The DC motors are driven and controlled with an off-the-shelf system manufactured by nuLogic. The nuDrive™ is a complete power amplifier and system interface unit for up to four axes of servo or stepper motion control. For servo motors, nuDrive™ utilizes PWM amplifiers with a user specified peak output current rating and a DC voltage. The front panel, Figure 9 contains both Power and Enable switches for direct motor inhibiting and system power down operations.

15

Figure 9.   Control panel of NPS 15" × 20" Flow Visualization Water Tunnel

The nuDrive™ unit is connected to a PC control board, which is a four axis servo motor control board that provides high performance motion control for IBM compatible computer systems. Each axis can be programmed for velocity, acceleration and position control in both continuous and point-to-point motion. Closed loop servo performance is fully programmable via a time sampled digital filter control loop. For dynamic tests, accurate motions are specified via software (LabView™) and the motion data, as well as the force/moment data, can be stored for later display and analysis. For simple flow visualization tests, the model support can be operated manually inside the software in the "Move Model" panel that allows changing the model position in any axis.

B.   DYE INJECTION

One of the simplest ways to visualize liquid flows is the use of colored dye in the study of complex three-dimensional flows over a delta wing. For the experimental set-up in the NPS 15" × 20" water tunnel, the colored dye is injected into the water tunnel flow from dye tubes inserted in to the leading edge of the UCAV 1303 model just beneath the surface of the wing. The path of the dye flow was carefully and meticulously manipulated

16

at the regions of the UCAV 1303 model to capture the required flow visualization information. Four ports were placed symmetrically on either side of the fuselage where two of the dye tubes are placed to capture the flow visualization around the critical region of the wing/body junction position. It is recognized that when the stream carrying the dye and all effects of dye injections are minimized only then will the true flow features revealed. Other methods include use of chemicals that initiate dye producing reactions at the desired points in the flow. For dye visualization to work correctly, the dye tubes interference were kept to be negligibly small since the released dye is contained in the wake of the tube. Efforts were made to prevent the wake from becoming unstable. When the wake becomes unstable, the turbulence of the wake diffuses the dye and proper visualization could not be achieved. The rate at which the dye released was ensured to match with the velocity of the stream around the UCAV 1303 model. If there is a large mismatch, the shear across the dye boundaries with the surrounding liquid could produce a totally different and unacceptable picture of the flow. For this case, the injection velocity should be minimized.

Food coloring used in the NPS 15" × 20" water tunnel was selected because it is readily available, inexpensive, neutrally buoyant, stable against mixing, provides good visibility contrast, non-toxic and non-corrosive.

It is observed that prolonged use of the food dye resulted in a build-up of dye in the water tunnel and thus, the flowing liquid has to be changed as soon as it becomes cloudy. During the course of the experiments, although the use of a bleaching chemical like Clorox will extend the operation time considerably, it uses are kept to a minimum because of the realization that it might corroded and damaged the gaskets and rubber seals of the water tunnel thereby causing leakage. The buoyancy was adjusted by diluting the concentrated food coloring with water. At high Reynolds number, it is necessary to be careful about the diffusion of the food coloring, since it can make the vortex collapse region less distinct.

C. CAMERA TRIGGER CONTROL SYSTEM

Since flow visualization images were required at various instantaneous angles of attack, and also, since the top- and side-views of the flow were recorded using two different cameras, it became necessary to devise a special arrangement to simultaneously document the flow pictures in a phase-locked manner. Figure 10 shows the schematic drawings of the phase-locked data acquisition system used for the maneuvering UCAV 1303 model unsteady flow images in the NPS water tunnel laboratory.
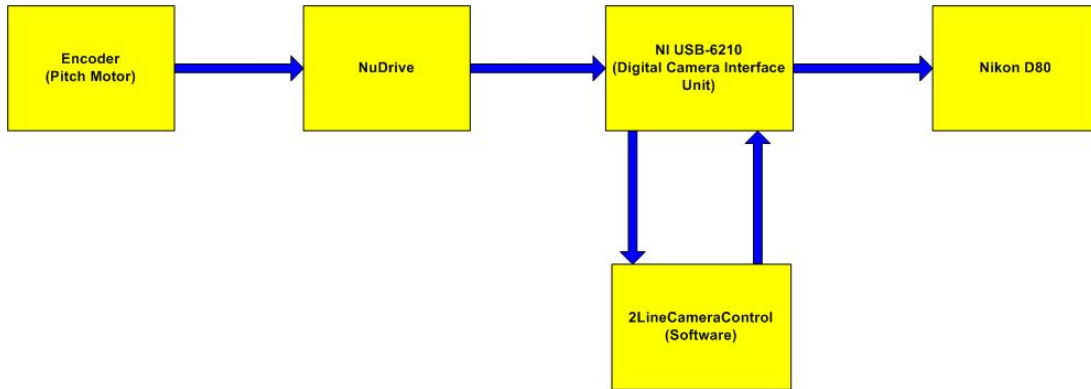

Figure 10.   Schematic of phase-locked data acquisition

The camera trigger control system consists of the modified Nikon D80 remote external shutter control MC-DC1 with a cable attached to the internal contacts, as shown in Figure 11.
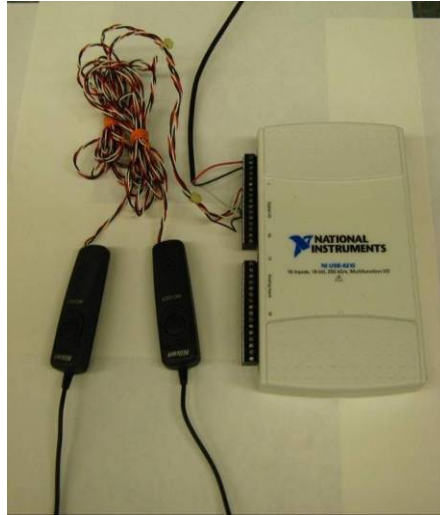
Figure 11.   Modified Nikon MC-DC1 hooked-up to Ni USB-620 digital converter

The motion-control software for the cameras uses Labview™ run-time engine and an executable program called "2LineCameraControl".

The NuDrive™ encoder inputs are monitored by the NI™ USB-6210 digital counter input port and resolved into degrees by the software. After the software has processed the input signals from NuDrive™, the data are relayed back to the unit where it sends out a signal to trigger the cameras at the pre-determined angle.

The "2LineCameraControl" software (Figure 12) considers the number of degrees between shutter operations, fine-tuned the number of "ticks" of the encoder to optimize synchronization of degrees read and then arm / disarm the shutters.

19

Figure 12.   Motion-control software, "2LineCameraControl", for the Nikon 80 cameras.

III. RESULTS

A. STEADY FLOW

Figure 13 and Figure 14 show typical flow visualization images obtained at angle of attack, $\alpha = 6°$ and angle of attack, $\alpha = 14°$ for Re $\cong$ 4,000. At this low velocity condition, the flow is laminar, and it is easy to see that for the case of angle of attack, $\alpha = 6°$, the flow exhibits remarkable symmetry. Also, the leading edge vortex has not formed in the region visualized, as can be inferred from the fact that the dye simply expands as it flows downstream, with the outer streaks being pushed towards the wing tips by the spanwise flow that develops on the wing. The slight lifting of the yellow dye in the side-view is believed to be due to the upstream effect of the nut on the sting.


Introduction of red-dye at wing underside
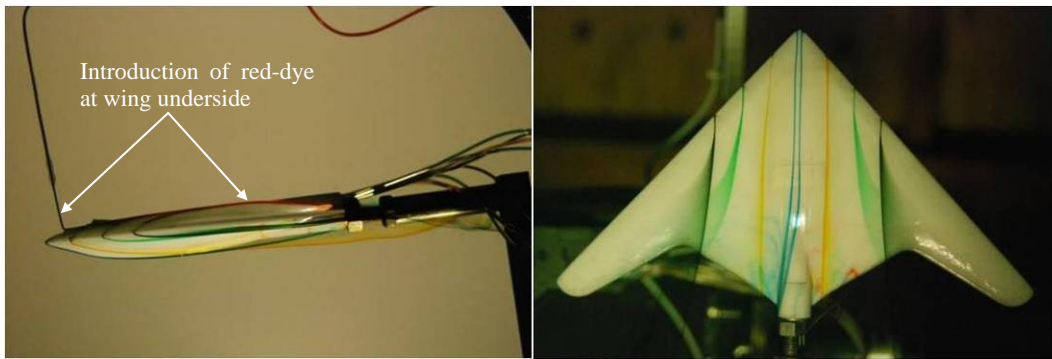
Figure 13.   Angle of attack, $\alpha = 6°$, Water tunnel velocity, U∞ = 2, [in/s], Re = 4.11×103
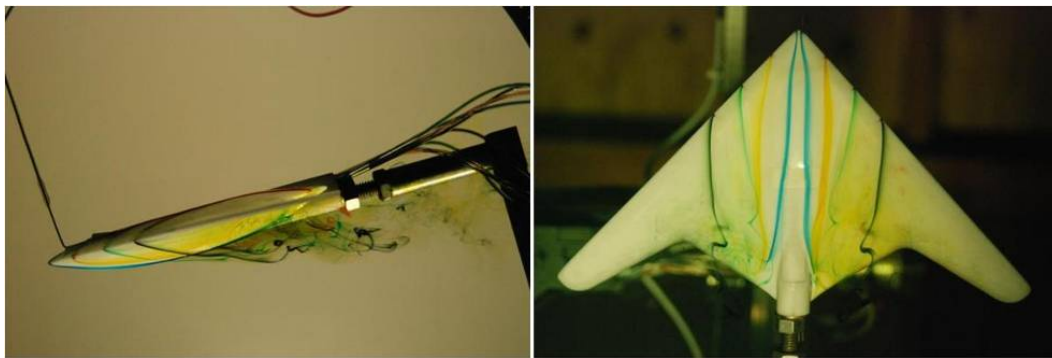
Figure 14.   Angle of attack, $\alpha = 14°$, Water tunnel velocity, U_∞ = 2, [in/s], Re = 4.11×10^3

In Figure 14, for the case of angle of attack, $\alpha = 14°$, the dye-streaks emanating from the same outer locations now flow towards the fuselage near the trailing edge crank location indicating a possible tip stall that is forcing them that way. Also, a symmetrical spiral breakdown is seen at about 80% chord.

## B.   EFFECT OF ANGLE OF ATTACK AT STEADY FLOW
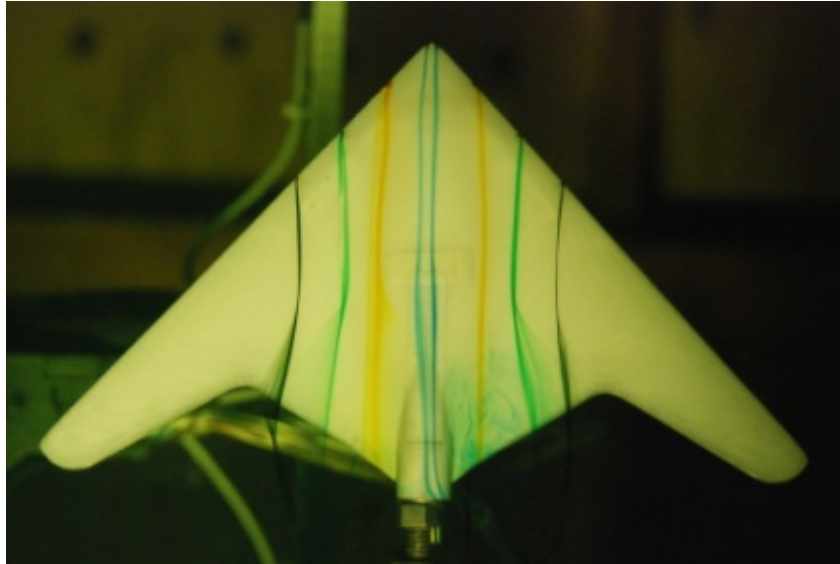
Figure 15.   Water tunnel velocity, $U\infty = 6$ [in/s], $Re = 1.24 \times 10^4$, angle of attack, $\alpha = 0^0$

Figure 15 presents the flow details at angle of attack, $\alpha = 0^0$ for a higher $Re = 12, 400$. Once again, exceptional flow symmetry can be seen. Some flow reversals appear to be present behind the cranked portion of the trailing edge around the engine / wing-body junction. As the angle of attack is increased from 0^0 to 6^0 (Figure 16, Figure 17 and Figure 18), the flow appears essentially similar to what was seen in Figure 13, with no separation other than possibly the tip stall mentioned above. The fuselage flow deviates slightly from the symmetry pattern; however, its displacement does not seem to have any preference as can be deduced from the blue-dye streak patterns. By angle of attack, $\alpha = 8^0$ (Figure 19), some asymmetry and a spiral breakdown is seen in the outer dye, but the inner flow appears to be essentially what was seen at lower angles of attack. There also appears to be some trailing edge flow reversals present, since the yellow dye is smeared locally.
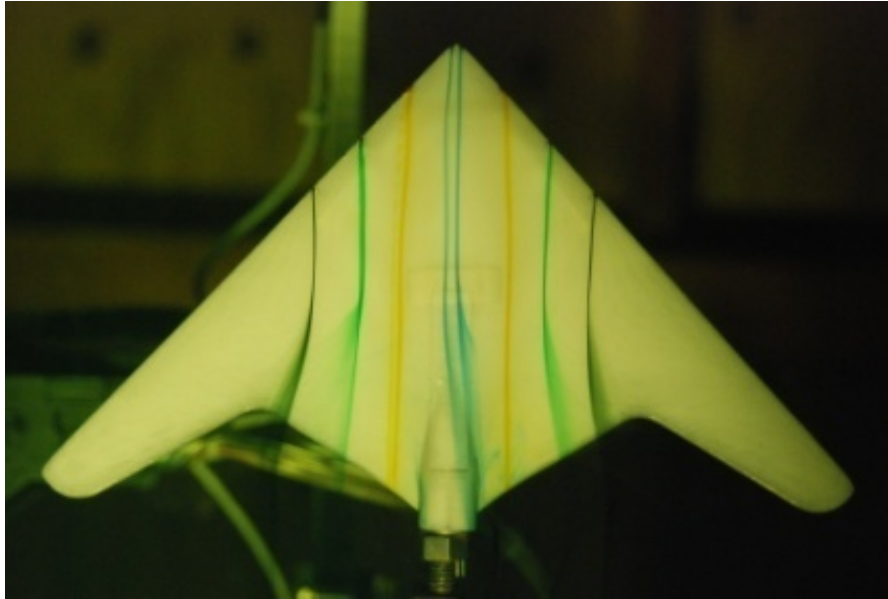
Figure 16.   Water tunnel velocity, U∞ = 6 [in/s], Re = 1.24×10^4, angle of attack, $\alpha = 2^0$
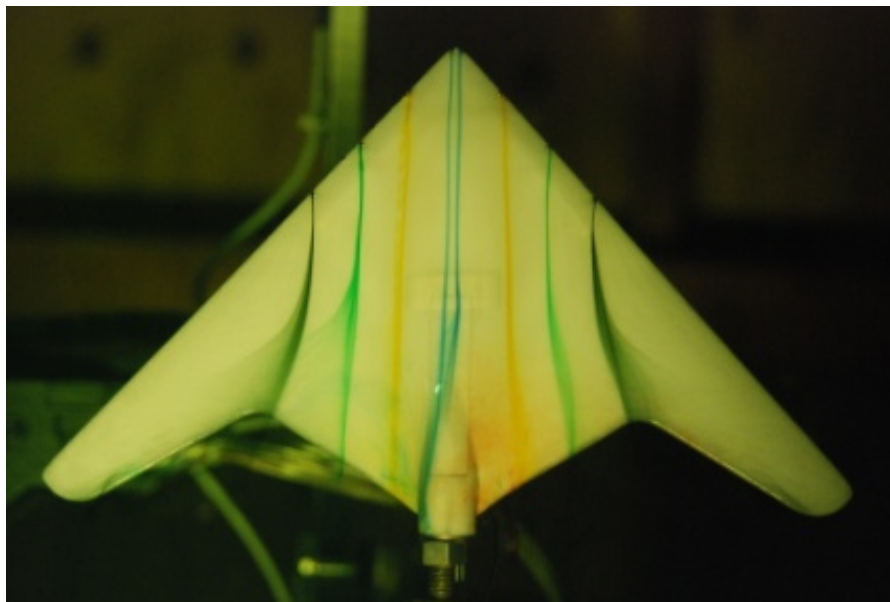

Figure 17.   Water tunnel velocity, U∞ = 6 [in/s], Re = 1.24×10^4, angle of attack, $\alpha = 4^0$
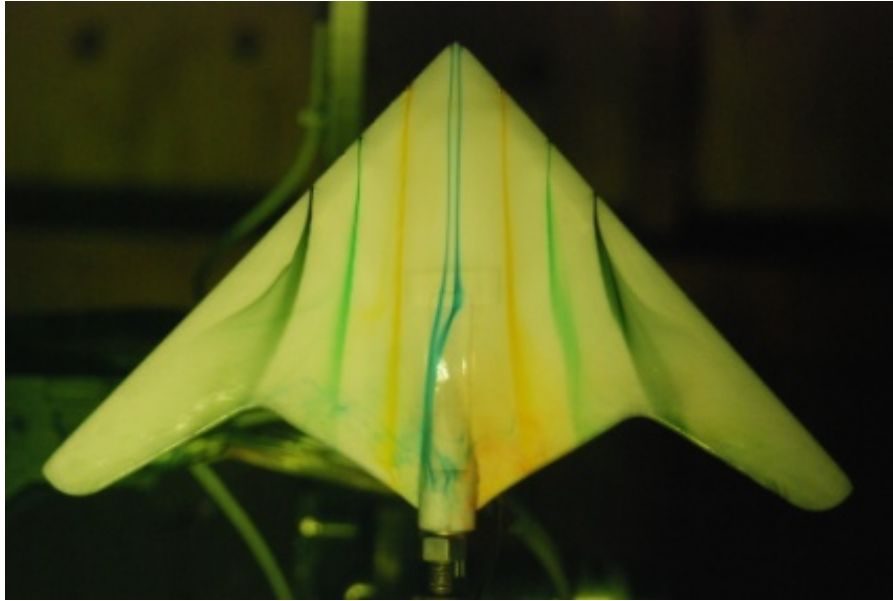
Figure 18.   Water tunnel velocity, U∞ = 6 [in/s], Re = 1.24×10^4, angle of attack, $\alpha = 6^0$
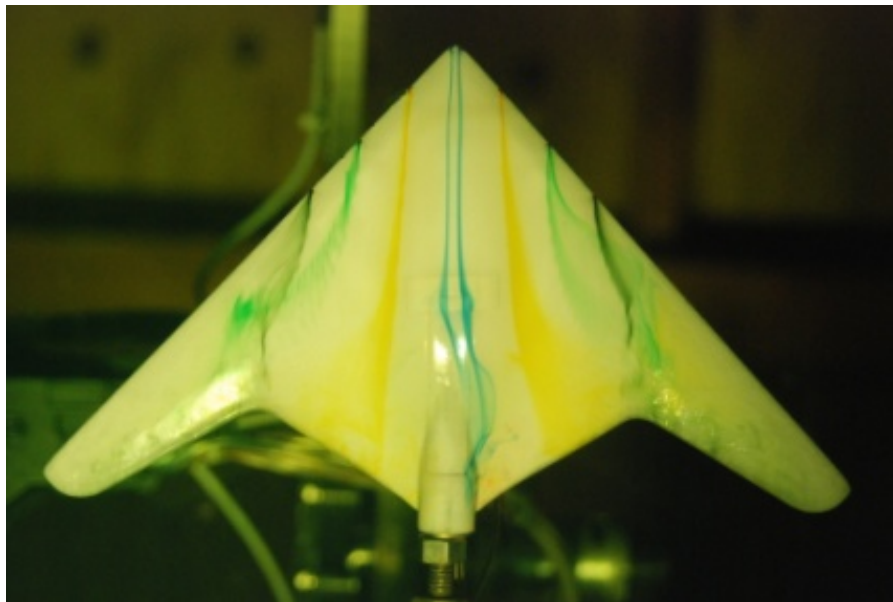


Figure 19.   Water tunnel velocity, U∞ = 6 [in/s], Re = 1.24×10^4, angle of attack, $\alpha = 8^0$
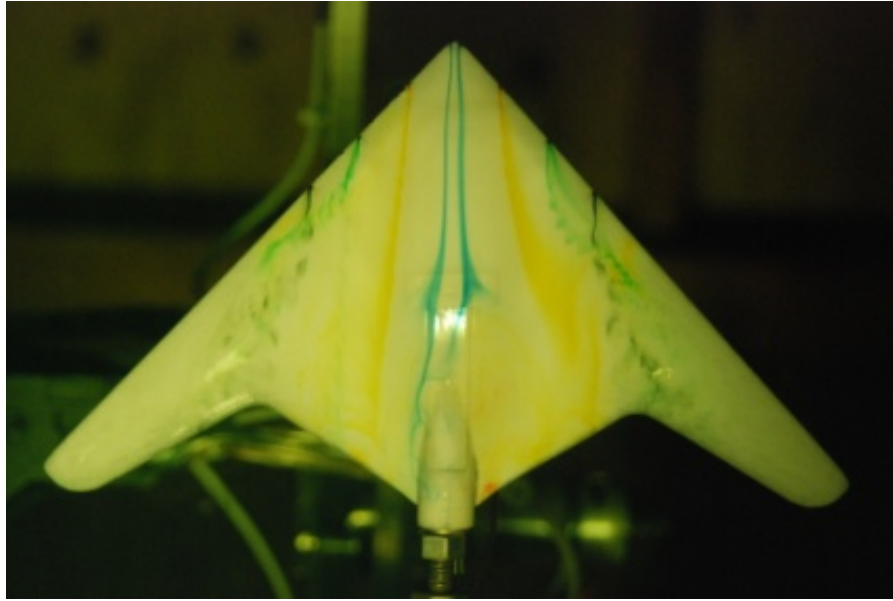
Figure 20.   Water tunnel velocity, U∞ = 6 [in/s], Re = 1.24×10^4, angle of attack, $\alpha = 10^0$

By angle of attack, $\alpha = 10^0$ (Figure 20 to Figure 23), the spiral breakdown pattern is found on the outer flow, as can be expected, since the effects of leading edge vortex have not been felt on the inner flow towards the fuselage on the port side. The flow over the fuselage, however, has encountered abrupt (bubble type) bursting on the starboard side, which also has caused the wing/body junction flow away from the fuselage and marked asymmetry has developed in the local flow (see blue dye). Beyond this point, (Figure 23 to Figure 26), the flow completely breaks down.
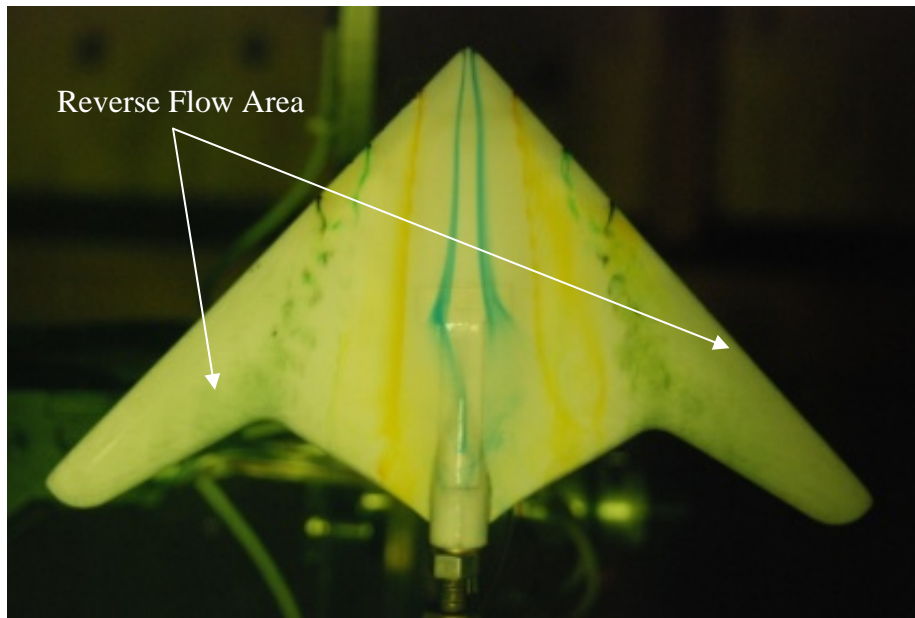
Figure 21.   Water tunnel velocity, U∞ = 6 [in/s], Re = 1.24×10^4, angle of attack, $\alpha = 12^0$
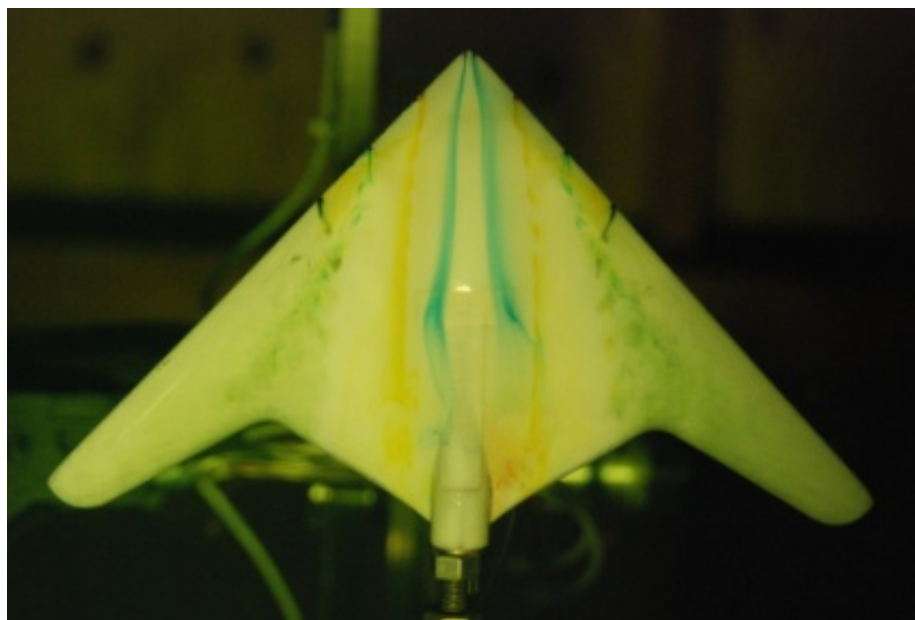
Figure 22.   Water tunnel velocity, U∞ = 6 [in/s], Re = 1.24×10^4, angle of attack, $\alpha = 14^0$
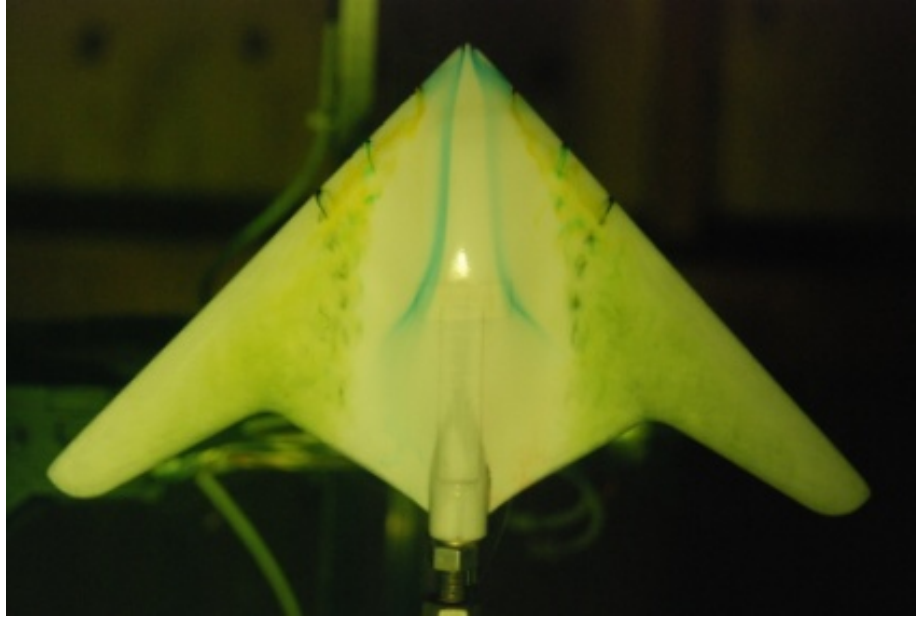
Figure 23.   Water tunnel velocity, U∞ = 6 [in/s], Re = 1.24×10^4, angle of attack, $\alpha = 16^0$
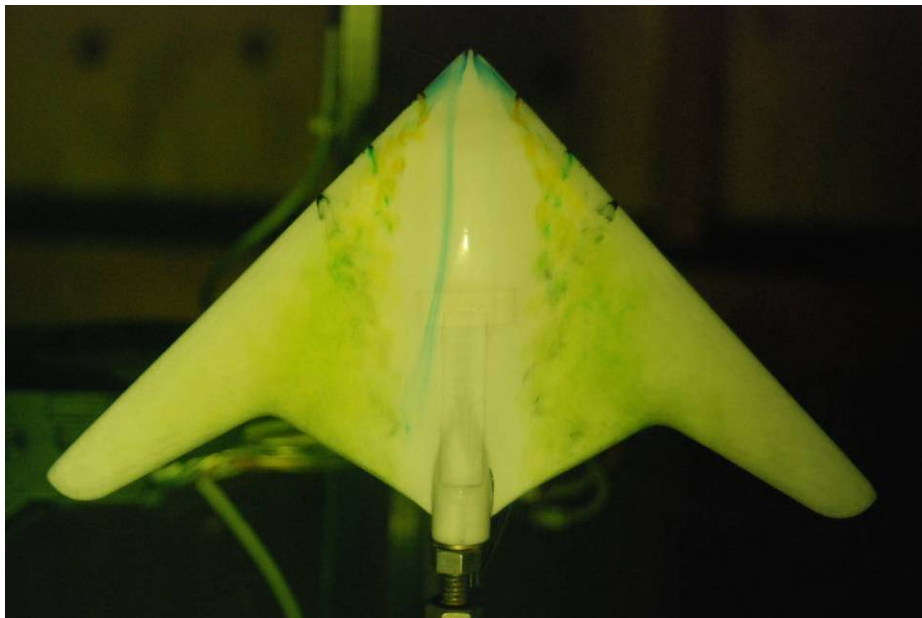
Figure 24.   Water tunnel velocity, U∞ = 6 [in/s], Re = 1.24×10^4, angle of attack, $\alpha = 18^0$
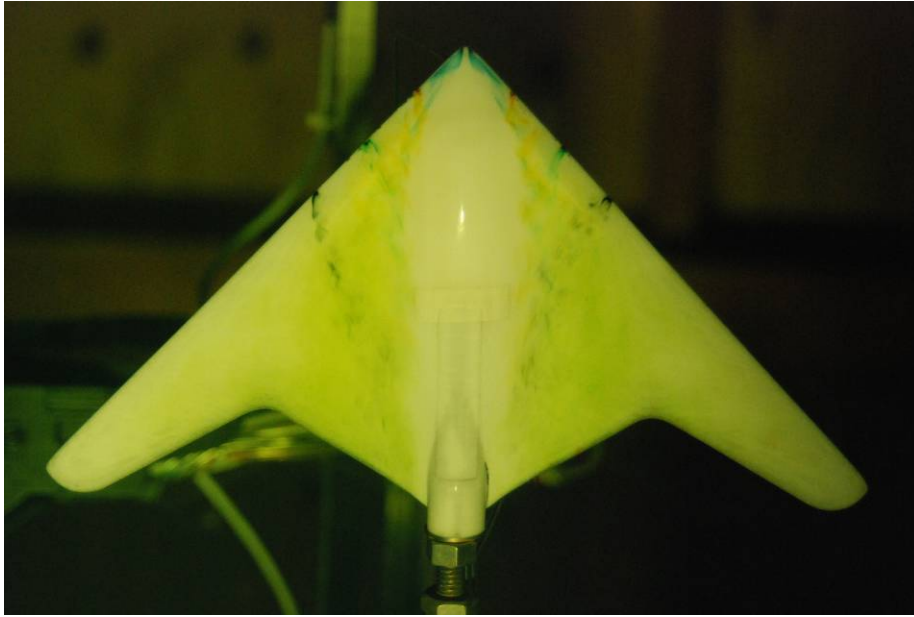
Figure 25.   Water tunnel velocity, U∞ = 6 [in/s], Re = 1.24×10^4, angle of attack, $\alpha = 20^0$
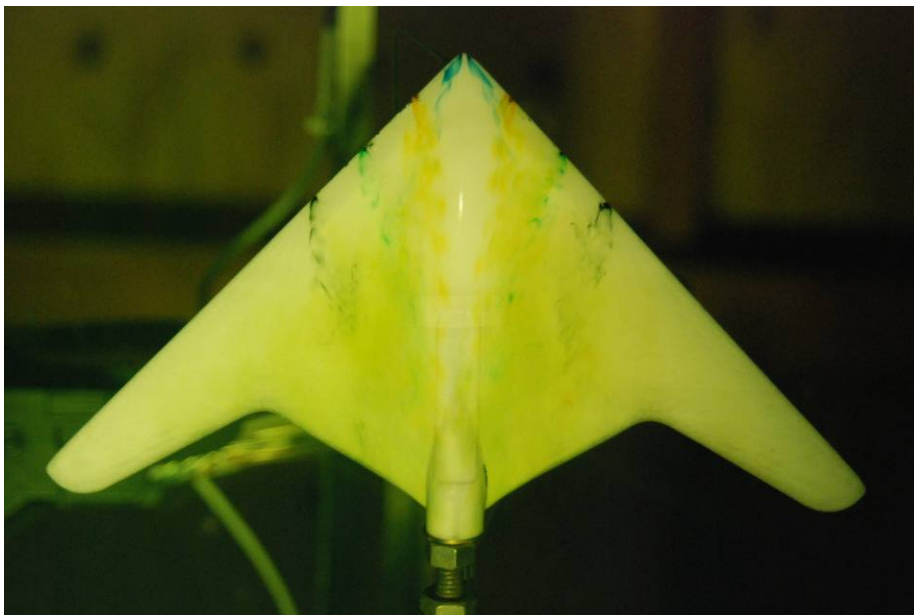
Figure 26.   Water tunnel velocity, U∞ = 6 [in/s], Re = 1.24×10^4, angle of attack, $\alpha = 22^0$

C. EFFECT OF REYNOLDS NUMBER, Re
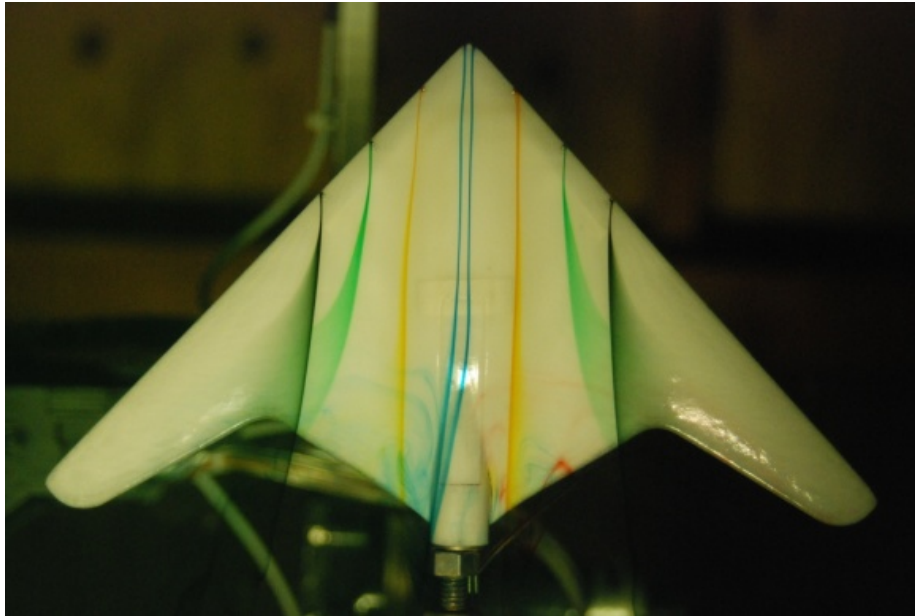


Figure 27. Water tunnel velocity, U∞ = 2 [in/s], Re = 4.11×10^3, angle of attack, $\alpha = 6^0$
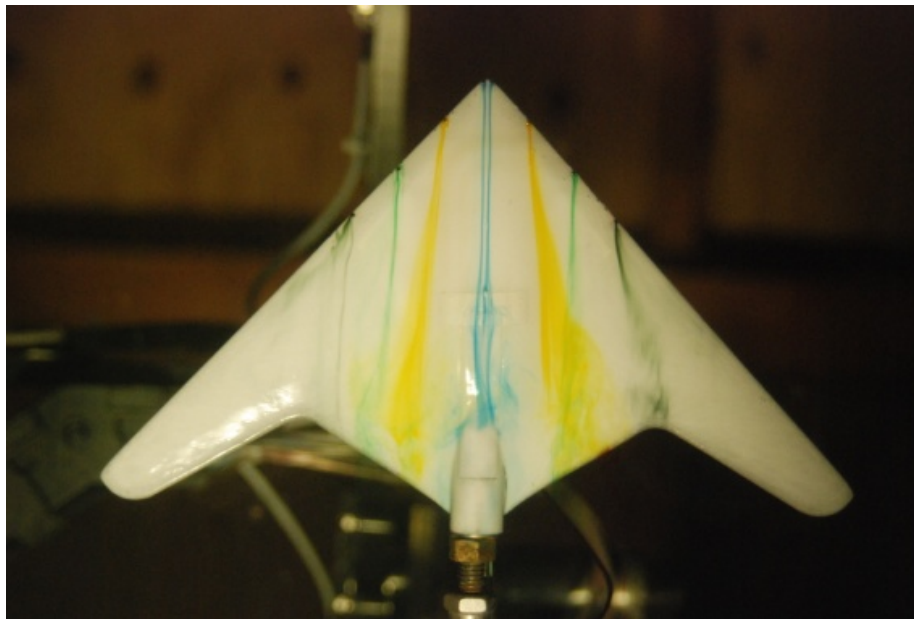
Figure 28. Water tunnel velocity, U∞ = 15 [in/s], Re = 3.08×10^4, angle of attack, $\alpha = 6^0$

The effect of Reynolds number is to promote vortex breakdown, which is easily seen in Figure 27 to Figure 30. At low Re, the flow is well behaved angle of attack, $\alpha = 6^0$, but the outermost portions of the flow are indicating vortex bursting at a higher Re. By angle of attack, $\alpha = 10^0$, the breakdown process has become quite severe at the higher Re.

In an effort to study the roll-up process, red-dye was introduced from the wing underside and in Figure 31, slight pooling of the red-dye can be seen, showing that there are pockets of re-circulating flow set up there. However, in the case of Figure 32, angle of attack, $\alpha = 12^0$, tip stalling appears to be present since the starboard tip is all red. Similar results are observed in Figure 33 and Figure 34.
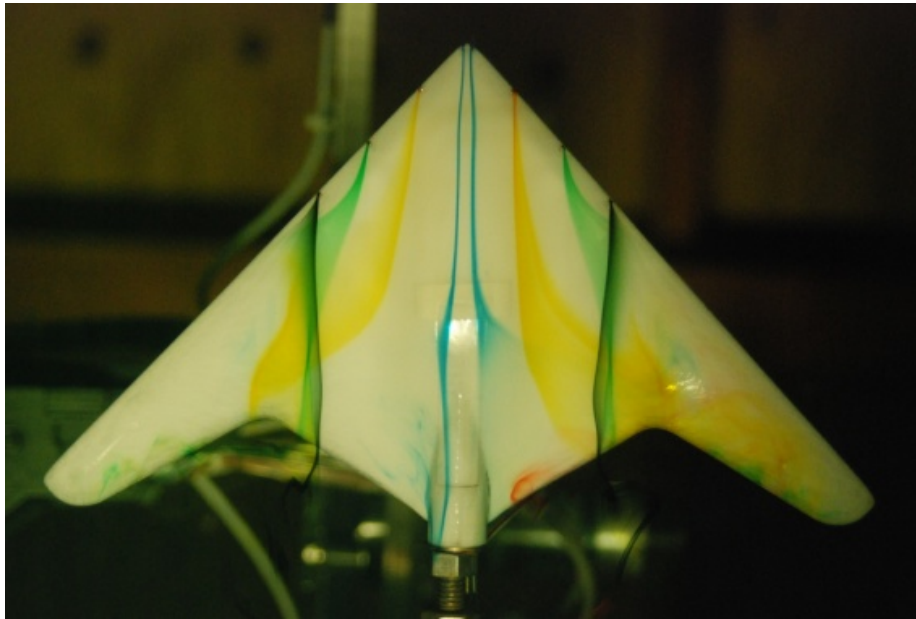

Figure 29. Water tunnel velocity, $U\infty = 2$ [in/s], $Re = 4.11\times10^3$, angle of attack, $\alpha = 10^0$
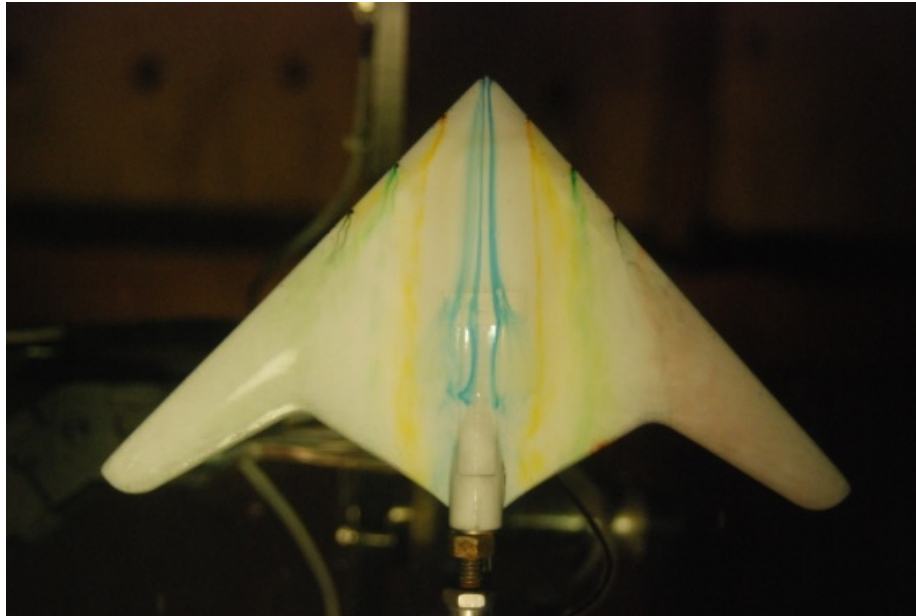
Figure 30.   Water tunnel velocity, U∞ = 15 [in/s], Re = $3.08{\times}10^{4}$, angle of attack, $\alpha = 10^{0}$

Introduction of red-dye
at wing underside
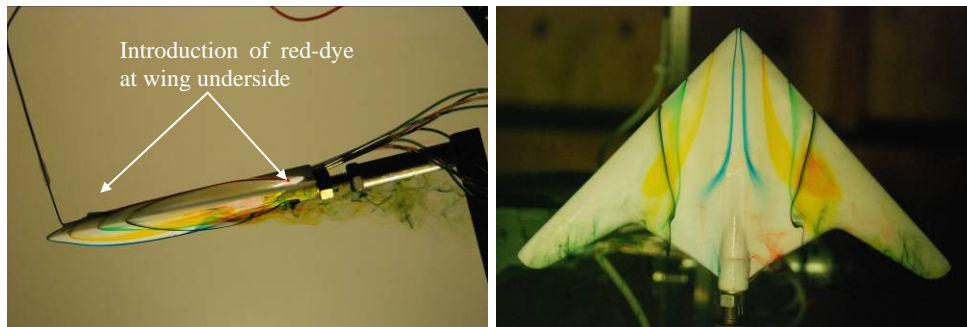
Figure 31.   Water tunnel velocity, U∞ = 2 [in/s], Re = $4.11{\times}10^{3}$, angle of attack, $\alpha = 12^{0}$
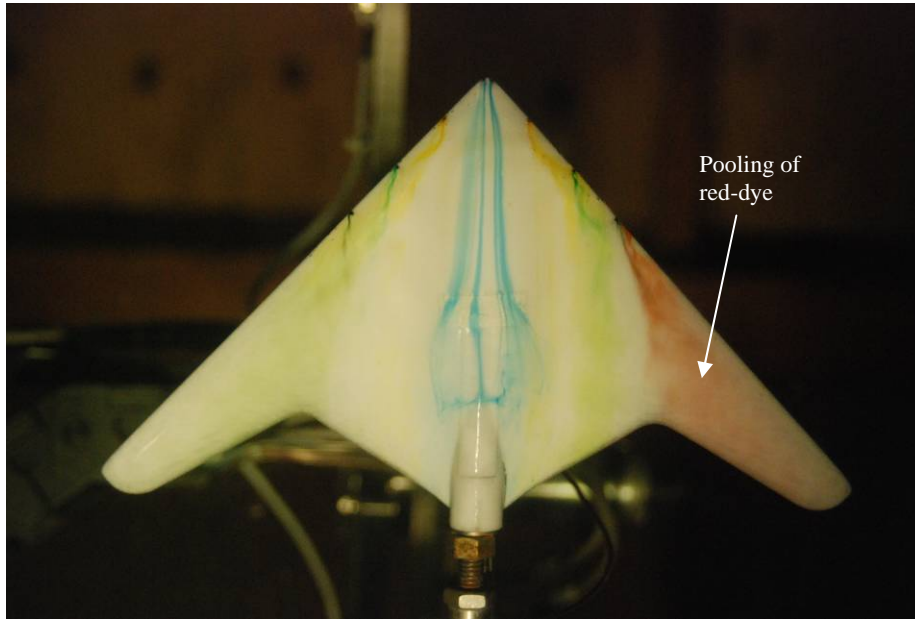
Figure 32.   Water tunnel velocity, U∞ = 15 [in/s], Re = $3.08{\times}10^{4}$, angle of attack, $\alpha = 12^{0}$
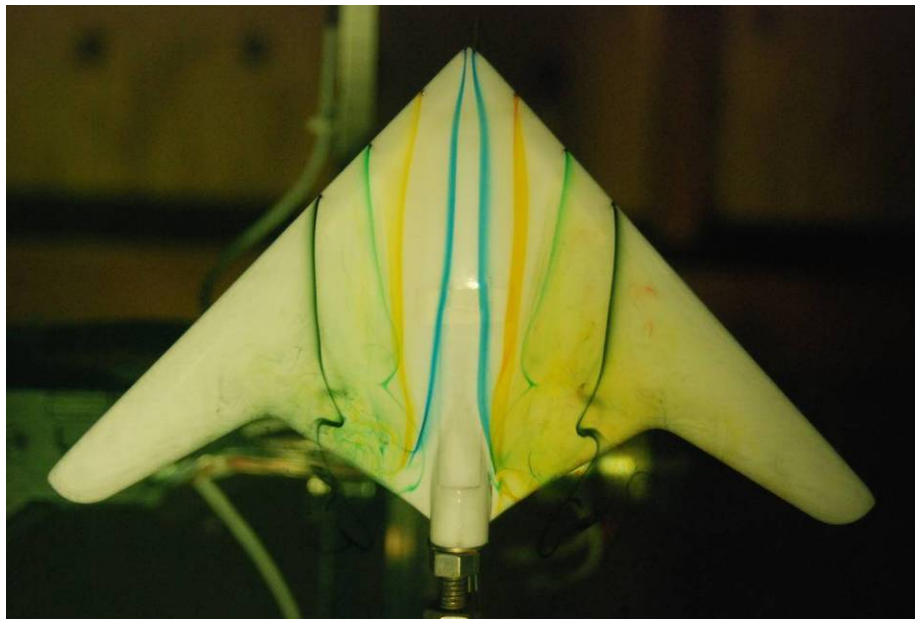
Figure 33.   Water tunnel velocity, U∞ = 2 [in/s], Re = $4.11{\times}10^{3}$, angle of attack, $\alpha = 14^{0}$
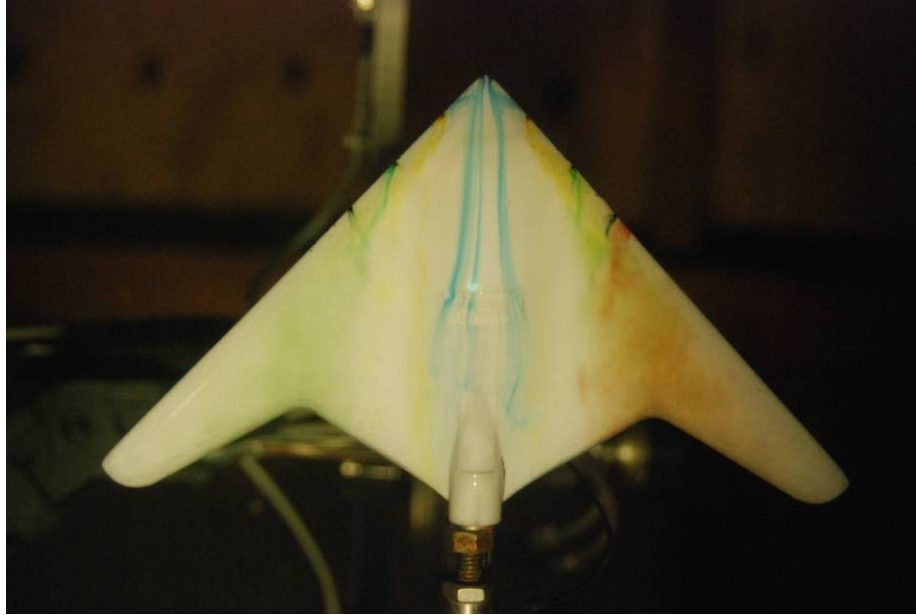
Figure 34. Water tunnel velocity, U∞ = 15 [in/s], Re = 3.08×10^4, angle of attack, $\alpha = 14^0$

D. UNSTEADY FLOW
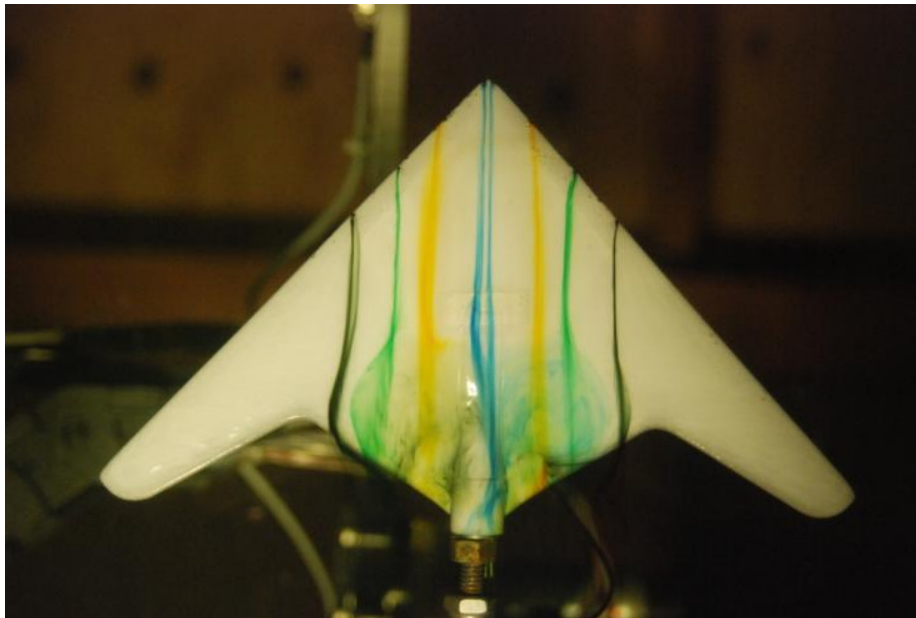
Figure 35. Vortices formation & breakdown at angle of attack, $\alpha = 6^o$, U∞ = 10 [in/s], Re = 2.05×10^4, non- dimensional pitch rate, $\alpha^+ = 0.05$
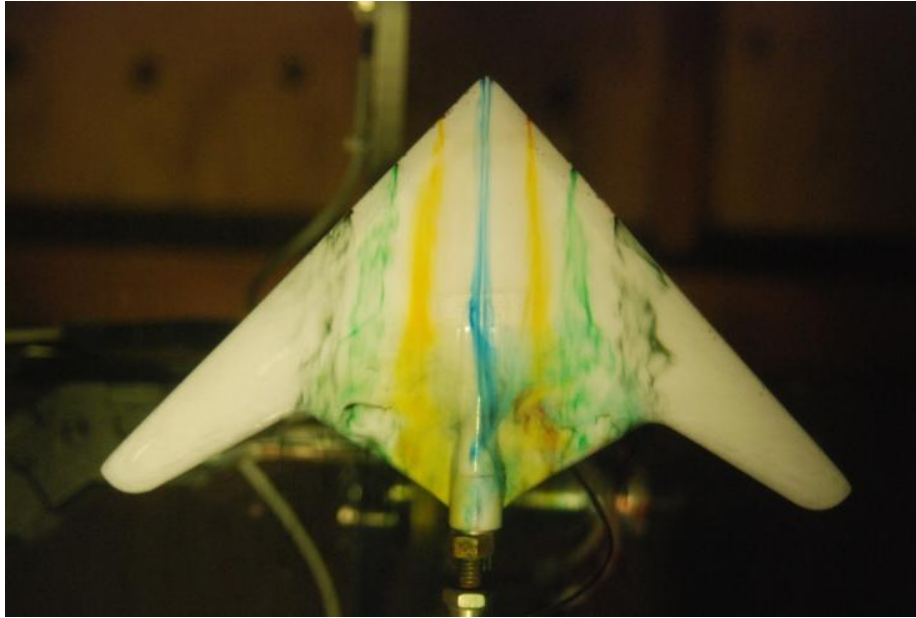
Figure 36. Vortices formation & breakdown at angle of attack, $\alpha = 14^o$, $U\infty = 10$ [in/s], Re = 2.05×10^4, non-dimensional pitch rate, $\alpha^+ = 0.05$
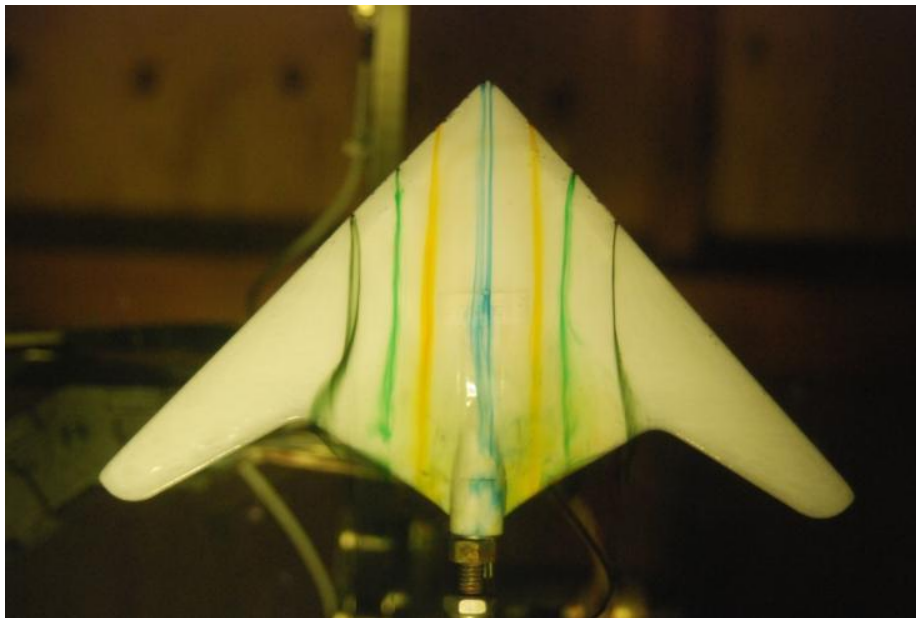
Figure 37. Vortices formation & breakdown at angle of attack, $\alpha = 6^o$, $U\infty = 10$ [in/s], Re = 2.05×10^4, non-dimensional pitch rate, $\alpha^+ = 0.1$
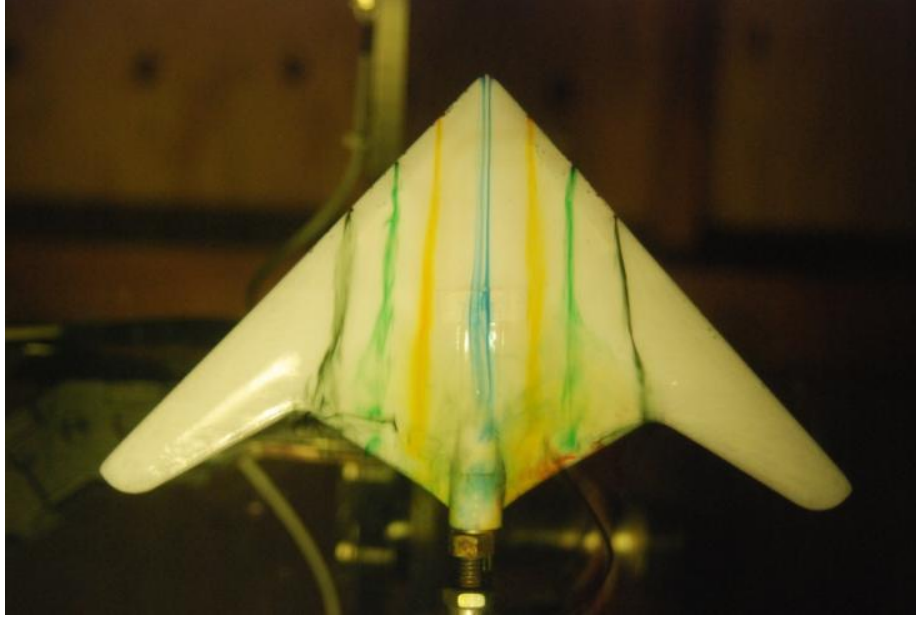
Figure 38. Vortices formation & breakdown at angle of attack, $\alpha = 14^o$, $U\infty = 10$ [in/s], $Re = 2.05 \times 10^4$, non- dimensional pitch rate, $\alpha^+ = 0.1$

It is well known that unsteadiness delays stall onset or vortex bursting. As a preliminary study, simple ramp tope pitching studies were conducted wherein the model was pitched from angle of attack, $\alpha = 0°$ to $40°$, at different rates defined by the non-dimensional pitch rate, $\alpha^+ = \dfrac{\dot{\alpha} U_\infty}{c}$, where $\dot{\alpha}$ is the dimensional rate of pitch, and the other variables have their usual meaning. It is clear from the reviews of Figure 34 to Figure 38 that at the same angle of attack and Reynolds number, increasing the unsteadiness from 0.05 to 0.1, delays the stall onset significantly.

E.   DISCUSSION OF RESULTS

1.   Vortex Collapse

Spiral and bubble vortex collapses are the two regular types of vortex bursting. From the experiments, spiral vortex collapse was observed. At $14°$ (Figure 22), the collapse took place at around $x/c = 0.4$ where spiraling motion was observed just before the collapse.

At 18° to 22° (Figure 24 to Figure 26), the location of the vortex collapse was difficult to estimate, but spirals are observed just before the collapse. Stagnation points are seen along the spanwise in the region of reverse flow where the bubble type vortex completely breaks down.

These observations proved that the spiral-type vortex collapse is the most common on the UCAV 1303 geometry.

2.   Flow Mechanics

From the recorded velocity of the water-tunnel at 6 in/s (0.15 m/s) and angle of attack at 6° (Figure 18), since the vortices strength increases with angle of attack, the vortex structure was not evidently observed, as well as the absence of vortex collapse over the wing of the UCAV 1303 model. The path followed by the dye is about a straight line with seemingly a low flow vorticity.

At 8° (Figure 19) and 10° (Figure 20), the flow can be expected to have a higher vorticity at the higher angles of attack because the higher lift generated infers that as vorticity increases, the angle between the vortex core axis and the wing surface increased as well. At 10° (Figure 20) the sub-structure is still there and has moved outboard.

At Re $\cong$ 4,000, flow visualization images obtained at angle of attack, $\alpha = 6°$ and $\alpha = 14°$ are shown in Figure 13 and Figure 14. It is observed that at angle of attack, $\alpha = 6°$, the flow shows very good symmetry because the flow is laminar at low velocity. In addition, the leading edge vortex has not formed in the region visualized as can be deduced from the fact that the dye simply expands as it flows downstream, with the outer streaks being pushed towards the wing tips by the spanwise flow that develops on the wing. It is assumed that because of the upstream effect of the nut on the sting, the slight lifting of the yellow dye in the side-view is seen.

It is further observed that for angle of attack, $\alpha = 14°$ (Figure 14), the dye-streaks flowing from the same outer locations has flowed toward the fuselage near the trailing edge crank location and a symmetrical spiral breakdown is seen at about 80% chord. This shows that a possible tip stall that is forcing them that way.

At a higher Reynolds number, Re, of 12,400, the flow visualization images obtained at angle of attack, $\alpha = 0^0$ is shown in Figure 15. Once again, very good flow symmetry can be seen. Some flow reversals are seen behind the cranked portion of the trailing edge around the engine / wing-body junction. As the angle of attack is increased from 0^0 to 6^0 (Figure 16, Figure 17 and Figure 18), with separation of flow except flow to possibly stall at the tip, it appears to be similar to what was seen in Figure 13. As inferred from the blue-dye streak patterns, the flow at the fuselage moves away slightly from the symmetry pattern where the flow displacement, however, does not seem to have any preference.   At angle of attack, $\alpha = 8^0$ (Figure 19) some asymmetry and a spiral breakdown is seen in the outer dye, but the inner flow appears to be essentially what was seen at lower angles of attack. There also appears to be some trailing edge flow reversals present since the yellow dye is smeared locally.

From the flow visualization images obtained at angle of attack, $\alpha = 10^0$ (Figure 20 to Figure 23), since the effects of leading edge vortex have not taken place on the inner flow towards the fuselage on the port side, then, as expected, the spiral breakdown pattern is found on the outer flow. Nonetheless, the flow over the fuselage has encountered abrupt (bubble type) bursting on the starboard side, which also has caused the wing/body junction flow away from the fuselage and from the flow path of the blue dye observed, marked asymmetry has developed in the local. The flow completely breaks down at angles of attack greater than angle of attack, $\alpha = 16^0$ (Figure 23 to Figure 26).

From Figure 27 to Figure 30, it is seen that the effect of Reynolds number is to promote vortex breakdown. At low Re, the flow is well behaved angle of attack, $\alpha = 6^0$, but the outermost portions of the flow are indicating vortex bursting at a higher Re. By angle of attack, $\alpha = 10^0$, the vortex collapse process has become quite severe at the higher Re.

From Figure 31, it is seen that there are areas of re-circulating flow at the underside of the wing from the slight pooling of the red-dye which indicates a roll-up

process. However, at angle of attack, $\alpha = 12^0$ (Figure 32), since the starboard tip shows an abundant of red dye stalling at the tip is deduced. Similar results are observed in Figure 33 and Figure 34.

From the flow visualizations images of Figure 34 to Figure 38, it is observed from a simple ramp tope pitching studies conducted at different non-dimensional pitch rate, $\alpha^+ = \dfrac{\dot{\alpha} U_\infty}{c}$, that the unsteadiness increased from $\alpha^+ = 0.05$ to 0.1 delayed the stall onset considerably at the same angle of attack and Reynolds number. This has further demonstrated the well known deduction that unsteadiness delays stall onset or vortex bursting.

Comparing to the results obtained with those from other experiments [8, 12] and CFD [15, 16, 17], the UCAV 1303 model used in this study was a scaled down but fully geometrically similar. The real UCAV 1303 has a three-dimensional shape, with in particular an increased thickness in the center part to house the engine, and an inlet just after the apex. It is obvious that these geometry differences have a strong influence on the flow development, especially in the centre part of the wing. The smaller scale UCAV 1303 model indicates a sharper leading edge but the flow over it is still similar

From experiments, the vortices seem to be developed at lower angle of attack, and more inboard. From the literature survey that when the Reynolds number decreases the vortex trajectory is shifted inboard and Reynolds number could be an explanation. The pressure distributions computed by CFD solvers show that the pitch break phenomenon is due to an increase of pressure on the outboard part of the wing [12, 18]. More exactly flow separation occurs near from the inboard crank, where the local chord is at a minimum, and produces a fully separated flow over the outboard part of the wing [9].

Comparing to the studies conducted by Wong [12], flow visualization at angle of attack, $\alpha = 12°$ (Figure 21) showed flow development on the CFD model is different from what was obtained. The main difference is the fact that the separation on the CFD model appears far from the apex, approximately at the span location, whereas in these experiments, the flow was separated from the apex. These differences could be due to the very low Reynolds number of the experiments.

Flow visualizations indicate that the vortex breakdown begins to occur over the wing at incidences higher than 12°. From Qinetiq force and moment measurements [13], the pitch up appears around 8° and even at angles of attack as low as 6° with the sharp configuration. Since pitch break takes place at higher angle of attack, it is one of the main reasons when the displacement of the vortex collapses over the wing. Therefore, it is inferred that the pitch up phenomenon is independent of the vortex breakdown displacement [13]. There are no significant changes in the flow structure or velocity at this range of incidence, apart from the strong outflow observed and moving forward with increasing incidence. This outflow could be responsible for a loss of peak suction on the outboard part of the wing, as it is the case for the CFD computations, and is hence supporting the hypothesis of a tip stall generating the pitch break [12].

THIS PAGE INTENTIONALLY LEFT BLANK

IV. CONCLUSION

A. SUMMARY

This flow visualization study has been useful to gain a first understanding of the flow features over these low swept wings, but as is well known, it can only provide a qualitative view of the flow. From literature researches, since the flow visualization cannot be used to accurately quantify the flows over the UCAV 1303 model, velocity fields measurements are recommended as a method to determine the influence of the trailing edge instead [14].

It is observed that flow over the UCAV 1303 model is complex with multiple vortices present even under steady conditions. Vortex busting occurs at higher angle of attack for low Re (steady flow) and is delayed with increase in pitch rate (unsteady flow).

To improve aerodynamic lift, delay vortex busting as much as possible, flow visualization studies gives the first insight on the maneuverability of a UCAV by observing the location and the time of vortex bursting. It is noted that a non-dimensional pitch rate of $\alpha+ = 0.1$ corresponds to about 3000 deg/sec pitch-up for a full scale aircraft, which is impossible if piloted.

From the experiments, it is inferred that flow visualization unlike pressure distributions, cannot be used to determine the pitch break physical explanation. But, it serves as a valuable tool to assess the qualitative flow features well. The results obtained are different from experiments done in the wind tunnel because the vortex development is different and the comparison between the effects of vortices on the surface pressure distribution between the water tunnel experiments and the wind tunnel tests are lest speculative [19]. In addition, in wind tunnels testing, quantitative flow visualization studies are inconclusive and are more suitable for demonstration than for comprehensive scientific research [19].

B.   FUTURE WORK

1.   Steady Flow

To continue with the qualitative studies at different water tunnel velocity for different roll and yaw angles

2.   Unsteady Flow

To continue with the qualitative studies at different water tunnel velocity for different roll and yaw angles, and the non-dimensional pitch rates, and to conduct unsteady pitch-up maneuver studies, acquire load data as ensemble averages. Further generation, analyze steady and unsteady flow aerodynamic performance.

LIST OF REFERENCES

[1]   S. J. Woolvin, UCAV Configuration and Performance Trade-offs, AIAA 2006-1264, 2006.

[2]   S. J. Woolvin, A Conceptual Design Study of the 1303 UCAV Configuration, AIAA 2006-2991, 2006.

[3]   G. S. Taylor, T. Schnorbus, I. Gursul, An Investigation of Vortex Flows over Low Sweep Delta Wings, AIAA 2003-4021, 2003.

[4]   M. R. Visbal, Computational and Physical Aspects of Vortex Breakdown on Delta Wings, AIAA 95-0585, 1995.

[5]   P. Gasquez, "Uninhabited Combat Air Vehicle Aerodynamics," M. S. thesis, Cranfield University, England. 2006.

[6]   R. M. Cummings, S.A. Morton, S.G. Siegel, Computational Simulation and PIV Measurements of the Laminar Vortical Flowfield for a Delta Wing at High Angle of Attack, AIAA 2003-1102, 2003.

[7]   J. Luckring, Reynolds Number and Leading-Edge Bluntness Effects on a $65°$ Delta Wing, AIAA 2002-0419, 2002.

[8]   K. Petterson, Low-Speed Aerodynamic and Flowfield Characteristics of a UCAV, AIAA 2006-2986, 2006.

[9]   S. C. McParlin, R.J. Bruce, A.G. Hepworth, A. J. Rae, Low Speed Wind Tunnel Tests on the 1303 UCAV Concept, AIAA 2006-2985, 2006.

[10]   U.S. Military Standard Weight and Balance Data Reporting Forms for Aircraft (including rotorcrafts), MIL-STD-1374A.

[11]   B. Tranchero, R. Bargetto, Neural Network-Based Approach to the Estimation of the Basic Mass Empty, AIAA 99- 0112, 1999.

[12]   D. W. Wong, G. J. McKenzie, M. V. Ol, K. Petterson, S. Zhang, Joint TTCP CFD Studies into the 1303 UCAV Performance: First Year Results, AIAA2006-2984, 2006.

[13]   R. J. Bruce, Low Speed Wind Tunnel Tests on the 1303 UCAV Concept, Qinetiq TR025502, 2003.

[14]   A. J. Smits, T. T. Lim, "Dye and Smoke Visualization" in *Flow Visualization Technique and Examples*, Imperial College Press, 2000, pp 43-69.

[15]   F. Zhang, M. Khalid, N. Ball, A CFD Based Study of UCAV 1303 Model, IAA 2005-4615, 2005.

[16]   K. Petterson, CFD Analysis of the Low-Speed Aerodynamic Characteristics of a UCAV, AIAA 2006-1259, 2006.

[17]   M. T. Aurthur, K. Petterson, A computational study of the low-speed flow over the 1303 UCAV configuration, AIAA 2007-4568, 2007.

[18]   M. D. Wong, J. Flores, Application of OVERFLOW-MLP to the Analysis of the 1303 UCAV, AIAA 2006-2987, 2006.

[19]   M. V. Ol, Water Tunnel Velocimetry Results for the 1303 UCAV Configuration, AIAA 2006-2990, 2006.

INITIAL DISTRIBUTION LIST

1. Defense Technical Information Center
   Ft. Belvoir, Virginia

2. Dudley Knox Library
   Naval Postgraduate School
   Monterey, California

3. Professor M.S. Chandrasekhara
   Department of Mechanical and Astronautical Engineering
   Naval Postgraduate School
   Monterey, California

4. Professor Yeo Tat Soon, Director
   Temasek Defence Systems Institute
   National University of Singapore
   Singapore

5. Tan Lai Poh (Ms), Assistant Manager
   Temasek Defence Systems Institute
   National University of Singapore
   Singapore